NASA Technical Memorandum 102822

# Natural Melting Within a Spherical Shell

Parviz A. Bahrami, Ames Research Center, Moffett Field, California

June 1990

National Aeronautics and
Space Administration

**Ames Research Center**
Moffett Field, California 94035-1000

# NOMENCLATURE

| | |
|---|---|
| $Ar$ | Archimedes number, equation (17) |
| $c$ | specific heat of liquid |
| $E$ | energy transfer, $E_\lambda + E_s$ |
| $E_s$ | energy transfer for sensible heat storage in liquid melt |
| $E_\lambda$ | energy transfer for melting |
| $E_{\lambda_{max}}$ | energy required to melt total mass in spherical shell |
| $Fo$ | Fourier number, equation (13) |
| $g$ | acceleration of gravity |
| $k$ | thermal conductivity |
| $M$ | melted mass |
| $M_{max}$ | total mass of phase-change medium in spherical shell |
| $Pr$ | Prandtl number, equation (17) |
| $R_i$ | inner radius of spherical shell |
| $R_o$ | outer radius of spherical shell |
| $s$ | solid travel distance |
| $Ste$ | Stefan number, equation (14) |
| $t$ | time |
| $T_A, T_B, T_C$ | thermocouple temperatures |
| $T_{w,o}$ | temperature of sphere outer wall |
| $T_{w,i}$ | temperature of sphere inner wall |
| $T^*$ | melting temperature |
| $\overline{T}$ | bulk temperature of liquid melt |
| $V$ | volume |
| $z$ | vertical coordinate |
| $\alpha$ | thermal diffusity of liquid |
| $\lambda$ | latent heat of melting |
| $\mu$ | viscosity |
| $\xi$ | dimensionless solid travel distance, equation (17) |
| $\rho$ | density |

## SUMMARY

Fundamental heat transfer experiments were performed on the melting of a phase-change medium in a spherical shell. Free expansion of the medium into a void space within the sphere was permitted. A step function temperature jump on the outer shell wall was imposed and the timewise evolution of the melting process and the position of the solid-liquid interface was photographically recorded. Numerical integration of the interface position data yielded information about the melted mass and the energy of melting. It was found that the rate of melting and the heat transfer were significantly affected by the movement of the solid medium to the base of the sphere due to gravity. The energy transfer associated with melting was substantially higher than that predicted by the conduction model. Furthermore, the ratio of the measured values of sensible energy in the liquid melt to the energy of melting were nearly proportional to the Stefan number. The experimental results are in agreement with our theory set forth in an earlier paper.


## INTRODUCTION

The importance of phase-change processes in the space and terrestrial environments is ever more widely recognized. Although the idea of phase-change thermal energy storage is an old one and has been employed in many applications, its usefulness has been limited. The low thermal conductivity of nonmetallic phase-change materials (PCMs) accounts for low rates of heat transfer, while rigidity of PCMs solidified on heat transfer surfaces makes their direct transport almost impossible. In an earlier paper (ref. 1), a promising concept for thermal energy storage, transport and temperature regulation, was introduced. The concept proposed to combine the higher energy storage capabilities of materials undergoing change of phase with the high effective thermal conductivity achievable in packed, fluidized, or moving beds of spheres. A sphere, referred to as a fusible sphere in this concept, consists of a spherical shell containing the phase-change material. The shell itself has a higher melting point than the phase-change medium. This enables cyclic melting and freezing of the phase-change material without any effect on its transportability, for example, in a moving bed. Alternatively, the spheres may be used in packed or fluidized beds, where they reside in hot or cold heat transfer fluids. In all such applications, the exterior surface of the sphere is heated causing inward melting of the medium during heat storage and cooled during extraction of energy, giving rise to its inward solidification.

Melting processes within spherical containments have been of fundamental interest, for example, in the well known Stefan and Neumann problems (refs. 2 and 3). The voluminous analytical literature on this subject, however, widely presumes that the yet unmolten part of the phase-change material remains at the center of the sphere. This is an unlikely occurrence in nature. The differing densities of the liquid and solid readily cause a force inbalance on the solid in gravitational and microgravitational environments, thereby moving the solid away from the center (fig. 1). Numerical results have been reported recently for the initial stages of melting and tests of a qualitative nature while movement of the solid was not restricted (ref. 4), and melting of a cold medium by a hot rigid sphere in a related problem concerned with magma migration and geophysics (ref. 5). Of particular relevance to the present work is the analysis of reference 6. Melting in a spherical shell while sedimentation of the solid occurred was investigated theoretically and a closed form solution was obtained. The present experimental results are in support of that theory.

Another issue stemming from the unequal densities of the solid and liquid materials is that they do not occupy a constant volume during phase change. Provision must therefore be made to accommodate the

volume changes. Most materials, with the notable exceptions of water, Gallium and some alloys, contract upon freezing. A rigid sphere fully filled with the liquid medium will be partially filled with the solid. Alternatively, elastic spheres will dilate upon melting of the medium if the solid had occupied the entire volume. Furthermore, due to the nonzero coefficient of thermal expansion of the liquid, additional volume increase is encountered when the temperature surpasses the melting point of the PCM. In the present study, free expansion of the phase-change material was permitted. A void sufficient for expansion of the medium was left within the sphere. The volume of the void was such that the liquid PCM occupied the entire volume of the spherical shell when the medium was at the highest boundary condition temperature encountered during the experimental runs.

Another notable difference between the present experiments and the classical approach to melting within containments is the imposition of a step function temperature jump on the outer shell wall in the present experiments. The inner wall is allowed to take whatever temperature the conduction and heat flow through the wall governs. The classical approach, however, would impose a step function temperature jump on the inner containment wall. The present choice of the boundary condition is appropriate, since we are concerned here with melting within a shell. The present experiments differ from those that may employ a highly conductive thin shell for the containment. In those cases, the inner wall temperature boundary condition would approach the outer wall temperature. Nevertheless, the resistance to heat flow through the shell material will always be present.

It is the focal point of this study to report results of melting experiments that allow natural movement within a stationary spherical shell. In principle, three convective mechanisms may accompany conduction within contained melting. The first mechanism is the flow of liquid resulting from the solid that is undergoing change of phase and simultaneously moving downwards toward the containment wall. The second and third mechanisms are flows due to expansion of phase-change material upon melting and natural convection driven recirculatory flows. These flows and close proximity of solid to the containment wall enhance the rate of heat transfer. A comparison of the results of the present experiments to the classical conduction model will reveal the extent of the enhancement of the rate of melting due to these processes.

## EXPERIMENTS

The phase-change material selected for the present experiments was 99% pure n-eicosane paraffin. Paraffins are noted for extremely low thermal conductivities. They are, however, stable, safe, noncorrosive and have large latent heats of melting. The freezing point of n-eiconsane is at 36 .4 °C (ref. 8). A spherical glass shell was especially blown for containing the paraffin in the experiments. Viewing of the solid-liquid interface was possible since n-eicosane is transparent in the liquid phase. The glass sphere was submerged in constant temperature water baths which served dual purposes. They provided the means of imposing the initial and boundary temperature conditions on the sphere. Furthermore, the water baths that had rectangular shapes substantially reduced the optical distortion due to differing indices of refraction of liquid paraffin and air. The timewise evolution of the melting process and the position of the solid-liquid interface was photographically recorded. Numerical integrations of the interface position data determined the amount of mass melted during each selected melting period. The component of energy input to phase-change was calculated. The sensible heat stored in the liquid melt as a result of temperature rise above the melting value was approximately determined from the temperature data reported by thermocouples inserted into the melt.

## Experimental Apparatus

The containment sphere for the phase-change material was a Pyrex glass spherical shell measured to be 72.9 mm in mean internal diameter and 1.7 mm in mean wall thickness. The sphere was constructed to a moderately high degree of sphericity and uniformity of wall thickness. It allowed excellent viewing of the phase-change material within it. The measurement procedure for the sphere dimensions will be described below. The sphere was supported by a stainless steel hollow shaft 6.4 mm in diameter and 45.0 cm long. A tube consisting of Pyrex and uranium glasses and a 5.0-cm-long Kovar shaft was used between the glass sphere and the stainless steel shaft. This arrangement was necessary to allow suspension of the sphere with sufficient strength and resistance to thermal expansion.

Two constant temperature water baths were constructed for imposition of the initial and boundary conditions. The first bath, which was used to establish initial temperature of the specimen, was a Plexiglass cubical container 30 cm on a side. A refrigerator, circulator, and controller were connected to this container in a closed loop flow. The spatial temperature uniformity within the bath was with 0.1°C of the preset value. The second constant temperature water bath was another Plexiglass container with dimensions of $30 \times 30 \times 45$ cm (width $\times$ height $\times$ length). This bath was used for imposition of the outer wall temperature boundary condition for each experimental run. This container was fitted with a heat-circulating unit capable of maintaining the water temperature with 0.1°C of the present value. Both Plexiglass containers were insulated with wool blanket insulation. Viewing of the containment sphere was possible through 20-$cm^2$ apertures in the insulation in the front and rear of the Plexiglass container. A circular fluorescent lamp provided lighting from the rear of the sphere. A sheet of ground glass diffused the light uniformly. A 35-mm single-lens-reflex camera was positioned on a tripod and looked horizontally at the sphere. This arrangement provided excellent silhouette photographs of the melting front.

Both water baths shared a common top plate that could be accurately positioned on either one by means of guide pins. The shaft supporting the sphere was attached to the top plate by means of a brass support flange. It provided a perpendicular shaft-plate configuration. The hollow shaft was held in a vertical position during the melting and freezing phases of the experiments. This was accomplished by means of levels positioned on the top plate and by adjusting the length of the legs under the Plexiglass containers. The entire experimental apparatus was positioned on a massive (300 kg) marble table equipped with vibration dampers.

Temperature measurements were made by a data logger capable of reading 0.1°C and were recorded at suitable time intervals. Two sets of thermocouples were used for temperature measurement. The first set, consisting of six Chromel-Alumel thermocouples, continuously monitored the temperature uniformity within the water baths. The second set, consisting of three Chromel-Constantan fine wire thermocouples, resided within the sphere for reporting the approximate bulk temperature of the melt. A more detailed description of their function will be given later.

In order to determine the degree of deviation of the glass shell from sphericity and uniformity of wall thickness, the external diameter of the sphere was measured at several points. The thickness of the sphere wall was also measured using an optical thickness measurement device. The sphere possessed excellent symmetry and uniformity of wall thickness in the planes perpendicular to the supporting shaft. The wall thickness varied by 0.2 mm with the maximum thickness of 1.8 mm residing around the neck of the sphere near the top, and also symmetrically near the bottom. The wall thickness gradually lessened to 1.6 mm at

the equator. The minimum external diameter measured from a point near the top to a point near the bottom was 75.2 mm. The maximum external diameter measured at the equator was 77.4 mm. The minimum and maximum internal diameters calculated from the above information were 71.6 mm and 74.2 mm, respectively. The maximum variation in the internal diameter was therefore approximately 3.6%. The mean values for the internal diameter and wall thickness, 72.9 mm and 1.7 mm respectively, are used in the data reduction procedure.

## Experimental Procedure

Initial preparation for the experiments included filling the glass sphere with molten paraffin, with the aid of the funnel attached to the hollow supporting shaft. The air being replaced by paraffin was removed by means of a stainless steel capillary tube inserted into the sphere through the hollow shaft and connected to a vacuum pump. The paraffin flow into the sphere, therefore, took place in the annular space between the shaft and the capillary tube. Clogging of the tubes by solidifying paraffin was prevented by application of heat from a heat gun. Sufficient paraffin was introduced into the sphere such that it was completely filled when the paraffin was held at a uniform temperature of 66 .4 °C.

Because air is soluble in liquid paraffin, cooling of the sphere was performed in a vacuum to prevent formation of voids in the solid specimen. The resulting solid was relatively void free, but possessed a crater-like upper surface. In order to start with a well defined upper surface, the sphere was taken out of the water bath and its upper part was heated with the heat gun. The crater-like surface was therefore melted into liquid paraffin. A void was generally present near the geometric center of the sphere. This void was also filled during the remelt operation. The sphere was then lowered into the initial condition bath that was held at 1°-2 °C below the melting point of the paraffin. Figure 2 shows the photographs of the melting evolution. The resulting solid specimen had a flat and horizontal top surface. Figure 2(a) is a photograph of the sphere taken a few seconds after the start of an experimental run. The flat upper surface is clearly visible between the air above and the solid PCM below. Following complete solidification, the temperature of the initial condition water bath was slowly increased and held at 36 .0 °C (slightly below the melting point to avoid melting of the impurities). The sphere was kept in this bath overnight to assure attainment of temperature uniformity. Meanwhile, the boundary condition bath was heated and maintained at 66 .4 , 56 .4 , or 46 .4 °C, pertaining to each of the three imposed boundary conditions.

The vacuum hose was removed from the sphere supporting shaft just prior to start of a run and the three fine-gauge thermocouples were carefully inserted through the hollow shaft into the neck of the glass sphere. The data logger was switched to print mode and the temperatures were measured and recorded in ten-second time intervals. An experimental run was started by lifting the top plate carrying the sphere and the inserted thermocouples from the initial condition water bath and lowering them into the boundary condition bath. The operation took less than five seconds. The establishment of the outer wall boundary condition was almost immediate. This constituted the start of the experiment running time. The camera was focused on the melt-solid interface and photographs were taken at one-minute time intervals. Slight oscillations in the temperature of the boundary condition water both ($\pm 0.5$°C) were observed due to the sudden introduction of the cold sphere at the start of the experimental runs. These oscillations disappeared quickly and the circulating water provided sufficient energy to maintain a uniform and constant sphere outer wall temperature.

Following accumulation of sufficient molten paraffin, the fine gauge thermocouples were lowered into the melt to report its approximate bulk temperature. The thermocouples were arranged to fan out into the melt. The tips of the thermocouples reported temperatures at a position located approximately in the center of the melt, and at positions progressively away from the center. They did not come in contact with the solid paraffin or the glass shell (figs. 2(c)-(i)).

## Data Reduction Procedure

The photographs taken during the evolution of the melting process, the recorded time, the bulk temperature of the melt, and the initial and boundary condition temperatures provided the basic information for data reduction. As evidenced in the representative photographs of an experimental run (figs. 2(a)-(i)), the outer boundary of the glass shell and the solid-liquid and liquid-air interface positions were clearly visible. The differing indices of refraction of air, glass, water, and liquid paraffin (index of refraction 1.44), caused an optical illusion in the photographs. The apparent thickness of the glass was amplified wherever the light beams passed through the water-glass-air system. The thickness, however, almost vanished in the water-glass-paraffin system. The solid paraffin in this case seemed to extend almost to the water-glass interface. When the tip of a fine wire thermocouple was placed in contact with the inside glass surface, the tip appeared to rest against the inner glass surface, showing a finite glass thickness if air constituted the inside medium. When liquid paraffin replaced the air, the tip appeared to be almost in contact with water. It was concluded that the photographs correctly indicated the close proximity of the solid paraffin with the inner wall of the glass sphere and that the melting layer was very thin.

Another concern with possible optical distortion of the position of the solid-liquid interface was resolved by examining the photographs of a linear scale submerged into liquid paraffin within the sphere and spanning the entire diameter. The departure from linearity was almost undetectable.

The photographs were enlarged so that the sphere diameter was 100.0 mm. The solid-liquid interface was then traced on graph paper (figs. 3-5). A fortunate outcome of the melting process, from the point of view of photographic evaluation of the unmelted mass, was the persistence of a convex upper solid surface for most of the melting periods. A side view, therefore, provided sufficient information for evaluation of the unmelted mass. Departure from this condition, aside from time = 0, occurred only during the very final stages of melting (<5% of the total mass still solid).

Description of the data reduction procedure will be facilitated with reference to the cylindrical polar coordinate system shown in figure 1. Taking advantage of the angular symmetry around the vertical axis of the sphere $z$, and denoting the horizontal distance from the $z$ axis outwards by $r$, the volume of solid PCM $V_s$ may be represented by

$$V_s = 2\pi \int_o^R r[z^*(r) - z_c(r)]dr \tag{1}$$

where $z^*$ is the height of the upper solid surface and $z_c$ is the height of the lower solid surface. Using the equation of a circle for $z_c$,

$$z_c(r) = R - (R^2 - r^2)^{1/2} \tag{2}$$

Equation (2) becomes

$$V_s = 2\pi \int_o^R r\left[z^*(r) - R + \left(R^2 - r^2\right)^{1/2}\right] dr \tag{3}$$

which may be expressed in summation form suitable for analysis of the tracings as

$$\overline{V}_s = 2\pi \sum_{n=1}^{100} n\left[\bar{z}^*(n) - \overline{R} + \left(\overline{R}^2 - n^2\right)^{1/2}\right] \tag{4}$$

where r is replaced by n and dr by 1. Values of $\bar{z}^*(n)$ were extracted from the traces of the solid upper surface on the graph paper. $\overline{V}_s$ and $\overline{R}$ also refer to the values in the photographs. In those cases where close angular symmetry was not observed, the arithmetic mean of $\bar{z}^*(n)$ values pertaining to left and right sides of the photographs was used. Equation (4) is valid only if the intersection of the solid upper surface and the sphere wall was below $\bar{z} = \overline{R}$. This condition was met for all cases except the totally unmolten case. For this case, the volume of the solid was calculated by determining the volume of the void space above the solid and by subtracting this from the theoretical value for the total volume of the sphere.

The volumes $\overline{V}_s$ were converted to $V_s$ values pertaining to the real dimensions of the glass sphere (2R = 72.9 mm) by applying the multiplication factor $(72.9/100.0)^3 = 0.387$. The agreement between the calculated hemisphere volume using equation (4) and the theoretical value based on the mean internal sphere diameter was better than 1%.

Denoting the total mass charge of paraffin in the sphere by $M_{max}$ and the volume of the totally unmolten paraffin by $V_{s_{max}}$, then

$$M_{max} = \rho_s V_{s_{max}} \tag{5}$$

Similarly,

$$M_s = \rho_s V_s \tag{6}$$

where $M_s$ is the mass of the solid paraffin at any instant of time and $\rho_s$ is the solid density. The mass of the total charge of paraffin, obtained by weighing the sphere before and after filling, differed from the $M_{max}$ value calculated from the photographic information by only a fraction of a percent. This lends support to the accuracy of the present mass evaluation technique.

The molten mass M at any instant of time is

$$M = M_{max} - M_s = \rho_s(V_{max} - V_s) \tag{7}$$

The energy absorbed in the melting of $M$ is

$$E_\lambda = \lambda M \tag{8}$$

and if the entire charge were to be melted

$$E_{\lambda_{max}} = \lambda M_{max} \tag{9}$$

It follows that

$$E_\lambda / E_{\lambda_{max}} = M/M_{max} = 1 - V_s/V_{s_{max}} \tag{10}$$

The approximate bulk temperature of the liquid region $\overline{T}$ was obtained by taking the arithmetic mean of the three inserted thermocouples

$$\overline{T} = 1/3(T_A + T_B + T_C) \tag{11}$$

where $T_A$ refers to the outermost thermocouple, $T_B$ to the middle and $T_C$ to the innermost thermocouple. Later, during the presentation of the results, it will be shown that the three thermocouple readings were within a couple of degrees of each other. The sensible energy $E_s$ transferred to the liquid melt is approximately

$$E_s = Mc\left(\overline{T} - T^*\right) \tag{12}$$

where c is the specific heat of the liquid.

The dimensionless groups which will be employed in presentation of the experimental results and in their comparison with the classical approach are the Fourier number, $Fo$, and the Stefan number, $Ste$. These are defined as

$$Fo = \alpha t / R^2 \tag{13}$$

$$Ste = c\left(T_{w,o} - T^*\right) / \lambda \tag{14}$$

in which $\alpha$ is the thermal diffusivity, $t$ the time, and $T_{w,o}$ is the outer temperature of the spherical shell. Later in comparison of the results with the analysis of reference 6, and experiments of reference 4, the mean inner wall temperature $T_{w,i}$ will be used in the definition of the Stefan number. This choice allows a more precise presentation and will be discussed later. The thermophysical properties $\alpha, c$, and $\lambda$ of liquid n-eicosane were valuated from information given in references 7 and 8.

## RESULTS AND DISCUSSION

The presentation of the results will begin with a discussion of the photographs of a representative experimental run. The evolution of the melting process for all imposed boundary conditions will be shown by the solid-liquid interface positions. The energies associated with melting of the solid and superheating of the liquid are then presented as functions of time. Finally, the results are correlated and generalized and a comparison with the classical conduction model of melting is made.

### Patterns of Melting

The patterns of melting within the sphere are clearly visible in figures 2(a)-(h). The photographs show the spherical shell described earlier, with the supporting glass shaft attached to the uppermost part of the sphere and extending vertically upward. Three distinct regions are visible within the sphere. The black lowermost region is the solid paraffin. The central region is the liquid paraffin, and the black upper region is the expansion space occupied by air. The lighting for all cases is from the back. The solid appears in black because it is opaque, whereas liquid paraffin is transparent and appears as a light region. Internal reflections on the inner surface of the glass sphere in contact with air are responsible for the black appearance of the air region. Also visible in figures 2(c)-(i) are the three fine gauge thermocouples which entered the glass sphere through the supporting shaft and resided within the liquid melt region.

Figure 2(a) was obtained a few seconds after the sphere was lowered into the boundary condition water bath. The melting process had just started, as evidenced by the straight horizontal line showing the initially flat upper surface of the solid paraffin. A thin layer of liquid paraffin on the upper solid surface and a few small air bubbles are also visible.

In figure 2(b), the molten region has expanded, occupying some of the space previously taken by the solid. The air volume above the liquid is also reduced due to expansion of the paraffin. Figures 2(c)-(h) show further progress in melting. Figures 2(a)-(h) correspond to the wall temperature $T_{w,o}$ = 46.4°C or the wall-to-melting temperature difference ($T_{w,o}$ - $T^*$) = 10°C. In figure 2(h), nearly all the paraffin was melted while the expansion space was not depleted. Figure 2(i), corresponding to another boundary condition temperature, shows the paraffin expanded into the entire glass sphere when held at 66.4°C. Figure 3, which is for the temperature difference ($T_{w,o}$ - $T^*$) = 10°C, conveys the results of figures 2(a)-(h) in the form of liquid-solid interface positions projected onto a vertical plane. Figures 4 and 5 are projections of interface positions corresponding to ($T_{w,o}$ - $T^*$) = 20, 30°C, respectively. In all cases, the solid mass was initially at the melting temperature.

Figures 3 through 5 show the position and shape of the melting front, starting at time = 0 and proceeding to longer times. Figures 3 and 4 contain information corresponding to six instants of time , while figure 5 contains information corresponding to seven instants of time. In all three figures, the upper boundary of the solid paraffin is indicated with the curves having a downward concavity, except for time = 0, which is a straight line. The lower boundary of the solid, aside from a thin melting layer, coincides with the glass shell wall. As indicated earlier, the optical properties of the system greatly diminish the apparent shell wall thickness. The air-liquid free surfaces are also shown in the above figures.

Inspection of figures 3 through 5 reveals that the pattern of melting is common to all three cases. The solid, having a greater density than the liquid, maintains a position in the lowest part of the containment sphere. The liquid, being more dense that air, takes a middle position with air remaining at the top. The sharp corners initially present at the intersection of the shell's inner boundary and the flat solid upper surface disappear in relatively short periods of time after the start of the experiments. The upper surface departs from a plane surface and assumes a dome-like shape. The general shape of the upper solid surface, however, remains relatively unchanged, while its height shrinks as time proceeds.

In order to place these findings in perspective, one may illustrate the differences between the findings of the present experiments and the classical viewpoint. If, in the absence of gravity and any disturbances, conduction were the sole heat transfer mechanism, then the solid would be expected to remain stationary with respect to the shell. Melting would take place primarily around the portions bounded by the sphere. Melting at the upper solid surface would proceed at a slower rate, owing to the poor thermal conductivity of air compared to liquid paraffin. The melting front might therefore be expected to resemble concentric spheres with truncated tops. Rounding of the upper solid corners might also be expected due to circumferential conduction in liquid. If expansion of paraffin were present, but the solid remained stationary, an accumulation of liquid paraffin above the top surface would be expected. Superheated liquid paraffin, having a greater thermal conductivity than air, would accelerate melting at the top.

In the present study, a significant departure from the above scenario is observed. The continuous close proximity of the solid to the containment wall assures a relatively high rate of heat transfer to the lower melting front. Furthermore, while liquid is generated at the solid paraffin's surface, the downward movement of the solid causes an upflow through the narrow region between the solid and the wall. Additional driving force is provided by the density decrease that accompanies melting. The liquified solid flows through the gap to seek more volume. The combined solid movement and volume expansion may amount to forced convention in the gap and in the free space above the solid. The displaced liquid may

cause melting to take place at the lower paraffin surface (in the gap) as well as the upper surface of the solid.

A close examination of figures 3 through 5 indicates that melting at the upper solid surface is much less rapid than melting at the lower solid surface. This is evidenced by the relatively unchanged shape of the upper surface after a short time (relative to duration of experiments). The height of the upper surface shrinks, primarily due to the diminishing lower solid mass and because the solid is supported from below.

## Melted Mass and Energy of Melting

The experimental data for the melted mass $M$ and the energy of melting $E_\lambda$ are presented in figure 6. These quantities are respectively plotted as dimensionless ratios $M/M_{max}$ and $E_\lambda/E_{\lambda_{max}}$ in that figure. Curves have been drawn through the data for the imposed wall-to-melting temperature differences $(T_{w,o} - T^*)$, 10.0, 20.0, and 30.0°C to depict continuity. The abscissa variable in figure 6 is the time in minutes. The melted mass and the corresponding energy of melting predictably increase with time and with the temperature difference $(T_{w,o} - T^*)$. The half melted state (i.e., $M/M_{max} = 0.5$) occurs after 15, 8, and 6 min of melting, respectively, for $(T_{w,o} - T^*) = 10.0, 20.0$, and 30.0°C. The numerical values indicate that the rate of melting varies somewhat nonlinearly with the temperature difference. Furthermore, the rates of melting for a given temperature difference decrease as melting proceeds. Several factors contribute to flowing the rates of melting. The primary factor is believed to be the decrease of the highly active lower solid-surface area which is in contact with the shell wall through the thin lower melting region.

Attention will not be focused on correlation and generalization of the results presented in figure 6. A technique is sought which would enable comparison of the present findings to the one-dimensional pure conduction model of inward melting. In that model, the density of the phase change material is assumed to be constant during melting and also superheating. The material, therefore, occupies the entire constant volume of the sphere. The geometry of the present experiments differs from the above, as described earlier. A direct comparison with the classical approach is, however, possible, as follows.

Suppose the paraffin mass $M$ contained in our experiments was held in a spherical containment of radius $R_i$. The void was a sphere placed entirely at the center of the containment. In the absence of gravity, spherically symmetric inward melting would result with the unmolten solid remaining at $T^*$ as time proceeds. Presence of the void, or in other words, lack of phase-change material at the center will be immaterial until the entire mass is melted. One may directly compare the rates of melting in the above scenario, pertaining to the classical approach, to the present experiments.

In figure 7, the melted mass and the energy of melting are incorporated within dimensionless parameters that emerge from the pure heat conduction model of inward melting. The dimensionless ratios $E/E_{\lambda_{max}}$ used in figure 6 are employed again but the abscissa variable is now the $Fo$ - $Ste$ product. The data in this figure are parameterized by $Ste$ rather than $(T_{w,o} - T^*)$. Essentially, $Fo$ is a dimensionless time and $Ste$ is a dimensionless form of the temperature difference $(T_{w,o} - T^*)$. The motivation for employment of the $Fo$ - $Ste$ product is two-fold. First, it enables assessment of how good or poor a correlation using the $Fo$ - $Ste$ product may be expected. Second, it facilitates a comparison between the data of the present experiments and the results of our earlier theoretical analysis. Enhancement or degradation of the rate of melting due to effects of solid movement and volume changes will then be apparent. Examination of

figure 7 indicates that employment of the $Fo$ - $Ste$ product has brought the data closer together than in figure 6, although a small spread in the data still exists.

Also appearing in figure 7 is the curve representing the numerical solution based on a one-dimensional heat conduction model of radially inward melting. This solution, obtained by Tao (ref. 3), incorporated the heat capacity of liquid in the numerical scheme. The results reported in reference 3 are only for $Ste = 0.1$, 0.5, 1.0.... The solid curve in figure 7 pertains to $Ste = 0.1$.

The experimental data lie above the predicted results of the one-dimensional pure conduction model. The maximum deviation is on the order of 100%. This deviation reflects the enhancement effect of the solid paraffin maintaining a close proximity with the shell wall (contrary to the one-dimensional model which assumes that the solid remains at the center). The data scatter in figure 7 may be attributed to the presence of additional resistance to heat flow in the shell wall. This issue will be revisited shortly during comparison of the results with our theoretical analysis.

The dashed curve shown in figure 7 is an overall representation of the data. A significant departure from the one-dimensional conduction model of melting is the nonasymptotic behavior of that curve at large values of the $Fo$ - $Ste$ product and, therefore, a finite time associated with complete melting.

## Sensible Energy Stored

The sensible energy $E_s$ stored in the liquid melt due to superheating of the paraffin above the melting point was calculated as described earlier. The information needed for this calculation included the mean bulk temperature of the liquid melt $\overline{T}$, which in turn was calculated from the thermocouple readings $T_A, T_B$, and $T_C$. Figure 8 shows these temperatures as a function of time with a continuous ordinate variable in degrees centigrade. Also shown in that figure are the constant temperature lines pertaining to the melting temperature of the paraffin $T^*$ and the imposed outer shell wall temperature $T_{w,o}$. The curves through the data points are the mean temperatures of liquid $\overline{T}$ (eq. 8). Figure 8 shows that the temperatures $T_A, T_B$, and $T_C$ in all cases were within 2° of each other and, in most cases, much closer. The upper liquid region appears to have been colder at the center and progressively warmer outwards. Furthermore, the mean temperature, $\overline{T}$, shortly after the start of each experimental run remained much closer to the shell wall temperature $T_{w,o}$ than to the melting temperature $T^*$.

It appears that most of the liquid, having traveled through the narrow lower liquid region and in contact with the shell wall, had acquired a temperature close to $T_{w,o}$. This is because the liquid formed at the melting temperature was forced through the narrow lower region for the length of its travel to the upper liquid region. There was apparently sufficient net heat input to increase its temperature to close to $T_{w,o}$. As time proceeded and the rate of heat transfer through the shell wall decreased, $\overline{T}$ and $T_{w,i}$ approached $T_{w,o}$ and eventually thermal equilibrium was established.

Although temperatures $T_A, T_B$, and $T_C$ remained generally close together, they signal a temperature gradient directed away from the solid paraffin surface. The higher fluid layers appeared to be warmer than the lower layers (adjacent to solid at $T^*$). It is, therefore, unlikely that strong natural convection flows were generated.

The liquid flow through the narrow region encountered a rapid increase in the flow area upon entering the upper liquid region. It may be speculated in view of the above that the upper liquid region was relatively stagnant, especially for the smaller wall-to-melt temperature differences. The heat transfer in this region was primarily governed by conduction.

The ratios of the sensible heat to the latent heat of melting, $E_s/E_\lambda$, as functions of time are presented in figure 9. Since the mean melt temperature $\overline{T}$ remained close to the shell wall temperature $T_{w,o}$, it is not surprising that the curves drawn through the data are almost horizontal. Moreover,

$$E_s/E_\lambda \sim Ste \tag{15}$$

Denoting the total energy input to the phase-change medium by $E$, then

$$E = E_\lambda + E_s \tag{16}$$

## COMPARISON OF THEORETICAL AND EXPERIMENTAL RESULTS

As pointed out earlier, only limited experimental data were available in the literature for comparison. In figure 10, data of reference 4 (circle and square symbols) have been recast in terms of the parameters of the present study. The solid curves in figure 10 are our analytical predictions (ref. 6) for the values of $Ste$, $Pr$, and $Ar$ pertaining to the above experiments. Where

$$\xi = \frac{s}{2R}, \quad Pr = \frac{c\mu}{k}, \quad Ar = \frac{\rho g(\rho_s - \rho)R^3}{\mu^2} \tag{17}$$

and $s$ is the downward distance the solid has travelled in time $t$.

The Fourier-Stefan product varies with $\xi$ according to the following relationship,

$$FoSte = \left(\frac{Ste}{PrAr}\right)^{1/4} \left(\frac{\rho_s}{\rho}\right) \left(1.56\xi + 0.279\xi^2 + 0.261\xi^3 - 0.0686\xi^4\right) \tag{18}$$

In recasting the data of reference 4 we have evaluated the fluid viscosity using the arithmetic mean of the wall and melting temperatures. Inspection of figure 10 reveals that use of $FoSte$ product instead of $Fo$ alone resulted in an improved correlation of the data by bringing the data together. The agreement between the theory and the experiments appears to be reasonable for small values of $FoSte$. The agreement is lessened for larger $FoSte$ values and the experimental data is approximately 20% below the theory.

While the theory presented in reference 6 is supported by the experimental data of reference 4, a more precise comparison cannot be made. Their numerical analysis makes cognizance of the solid-liquid density difference only so far as repositioning of the solid toward the base of the shell is concerned. As a result, the Archimedes number $Ar$ does not appear in their presentation. Furthermore, the resistance to heat flow in the glass shell was assumed to be negligible and reasonable agreement between the experiments and the numerical results was reported. Unfortunately, this assumption is not entirely valid. The temperature drop in the shell may amount to a fraction of the overall wall-to-melting-temperature difference. This would cause an overestimation of $Ste$ which should be based on spacially uniform and constant inner wall

temperature rather than the water bath temperature. The experimental data of reference 4 are, therefore, somewhat systematically shifted to the right. Another factor that may have contributed to the slower rates of melting than predicted in the present study is the absence of forced circulation and the limited heat capacity of the water bath used in the experiments. It may, therefore, be concluded that closer agreement between theory and experiments of reference 4 may be expected if more stringent boundary conditions were imposed.

In our experiments, as described earlier, the initial and outer shell temperatures were carefully controlled. The resistance to heat flow in the glass shell, however, was unavoidable. Close examination of the melting rates and the associated melting areas which are both functions of time, indicated that the spatially averaged temperature of the active portion of the inner shell remained relatively constant throughout each experiment. The mean temperature drop in the glass shell was, therefore, calculated using the melted mass, the active heat transfer area ($0 \leq \theta \leq \theta_A$), the time interval, and the information pertaining to the glass shell. The inner wall-to-melt temperature differences obtained with this method were 5.1, 8.3, and 15.8 °C, corresponding to $T_{w,o}$ values of 46.4, 56.4, and 66.4 °C, respectively. In the presentation of experimental results in figure 10, the approximate inner wall temperatures are used in calculation of $Ste$, while the fluid properties are evaluated at the arithmetic mean of the inner wall and melting temperatures. The results of the present experiments, triangles and diamonds, and the associated analytical predictions also appear in figure 10. Agreement between the experiments and the theory appears to be excellent for the slowest melting case. The agreement is, however, lessened for the faster melting cases. Factors such as uncertainty in the inner wall temperature and its spatial nonuniformity may be responsible. Although the present experiments utilize a truncated spherical solid to allow room for free expansion of the phase-change material, it appears that the present theory can be reasonably applied to predict the rates of melting and heat transfer in such cases.

## CONCLUDING REMARKS

Melting of a phase-change medium contained in a spherical shell and in the presence of gravity was significantly affected by movement of the solid toward the base of the sphere. The liquid generated in a thin melting layer between the inner shell wall and the solid medium was forced out to the top, assuring continued geometric conformity of the solid lower surface to the sphere. The melting at this region was much more rapid than melting at the upper surface due to the close proximity of the solid medium to the heated wall.

The experimental data for the melting-related energy transfer displayed much higher values than those predicted by a model based on concentric melting. The data were in agreement with the theory set forth in reference 6. The sensible energy of liquid melt was substantially smaller than the energy of melting and was nearly proportional to the Stefan number based on the outer wall temperature.

## REFERENCES


1. Bahrami, P. A.: Fusible Pellet Transport and Storage of Heat, ASME Paper 82-HT-32, 1982.

2. Carslaw, H. S.; and Jeager, J. C.: Conduction of Heat in Solids, Oxford University Press, Oxford 1959.

3. Tao, L. C.: Generalized Numerical Solutions of Freezing in a Saturated Liquid in Cylinders and Spheres, AICHE J., vol. 13, no. 1, 1967, p. 165.

4. Moore, F. E.; and Bayazitogh, Y.: Melting within a Spherical Enclosure, ASME J. Heat Transfer, vol. 104, Feb. 1982, pp. 19-23.

5. Emerman, S. H.; and Turcotte, D. L.: Stokes' Problem with Melting, International J. Heat and Mass Transfer, vol. 26, 1983, pp. 1625-1630.

6. Bahrami, P. A.; and Wang, T. G.: Analysis of Gravity and Conduction Driven Melting in a Sphere, J. Heat Transfer, vol. 109, no. 3, 1987, pp. 806-809.

7. Humphries, W. R.; and Griggs, E. I.: A Design Handbook for Phase Change Thermal Control and Energy Storage Devices, NASA TP-1074, 1977.

8. Hale, D. V.; Hoover, M. J.; and O'Neil, M. J.: Phase Change Materials Handbook, NASA CR-61363, 1971.

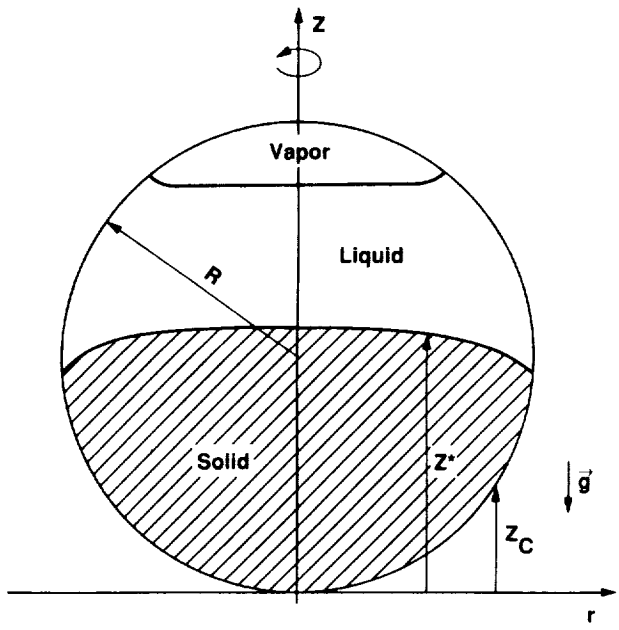


Figure 1. Melting in a cylindrical polar coordinate system.

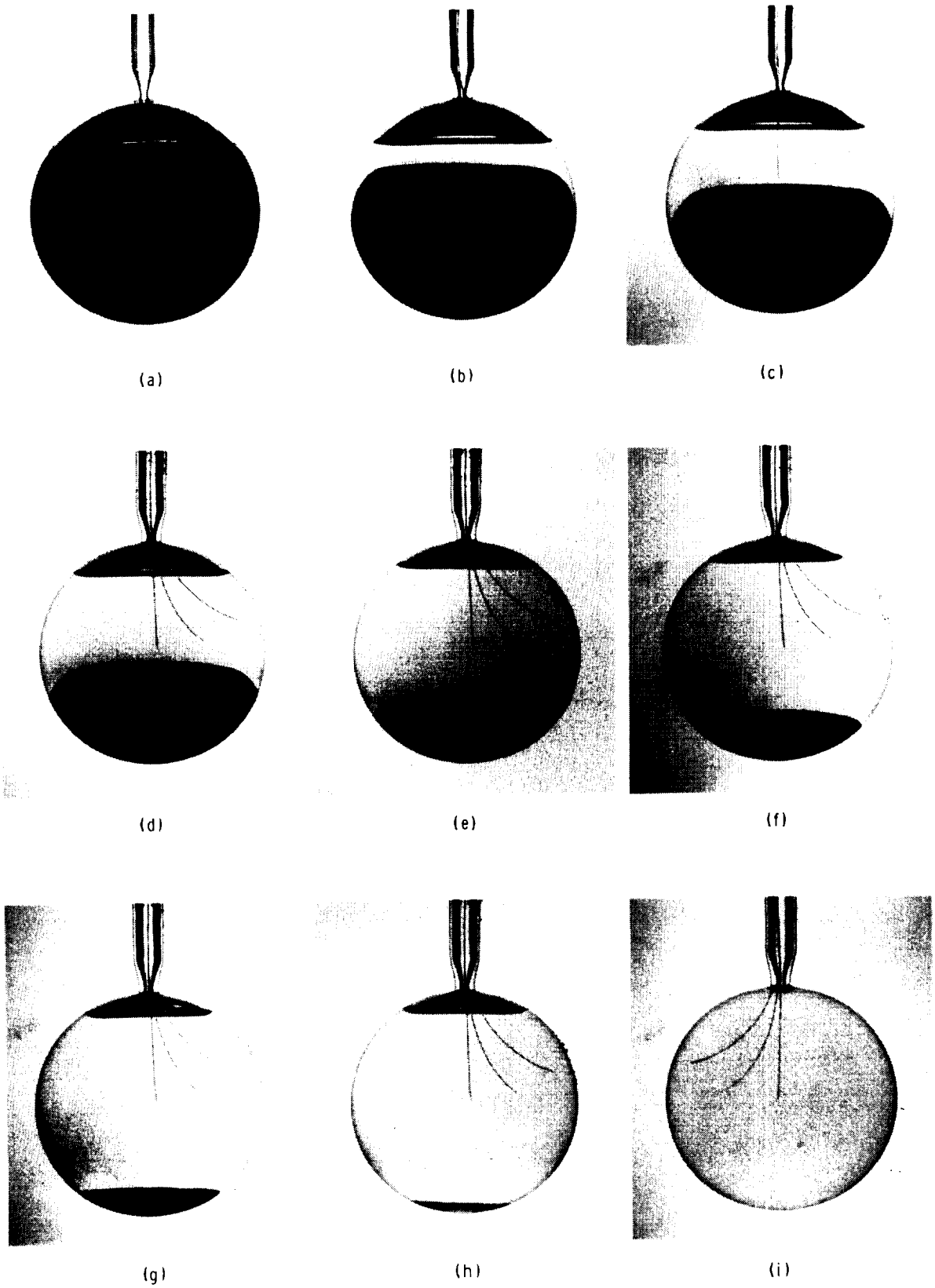


Figure 2. Photographs of n-eicosane melting evolution.

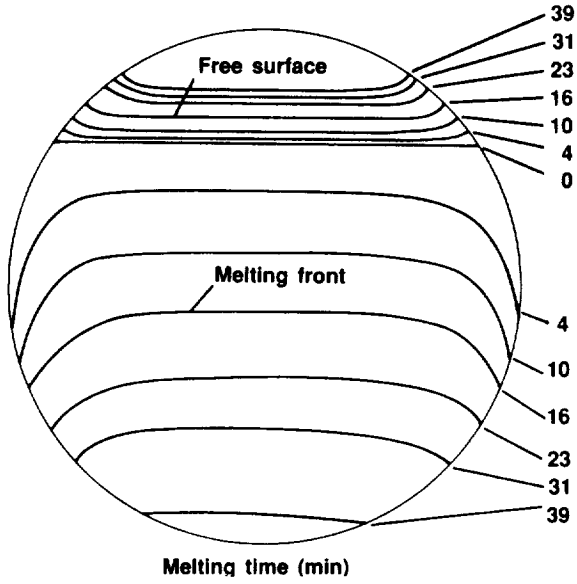


Figure 3. Position and shape of the melting front and the air-liquid free surface, $T_{w,o} = 46.4°C$.

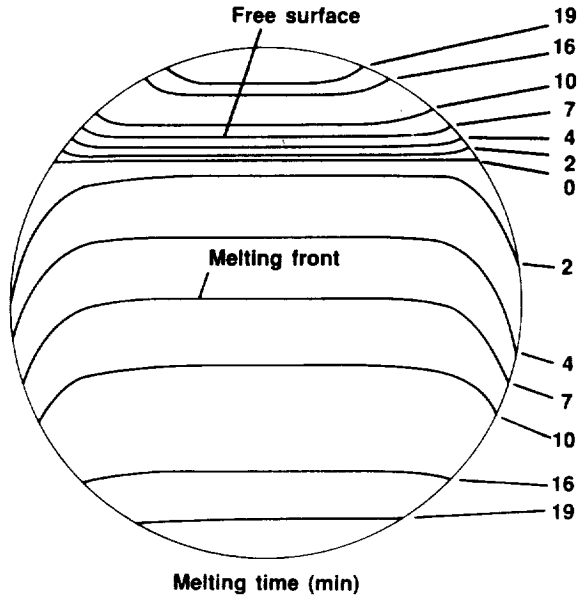


Figure 4. Position and shape of the melting front and the air-liquid free surface, $T_{w,o} = 56.4°C$.

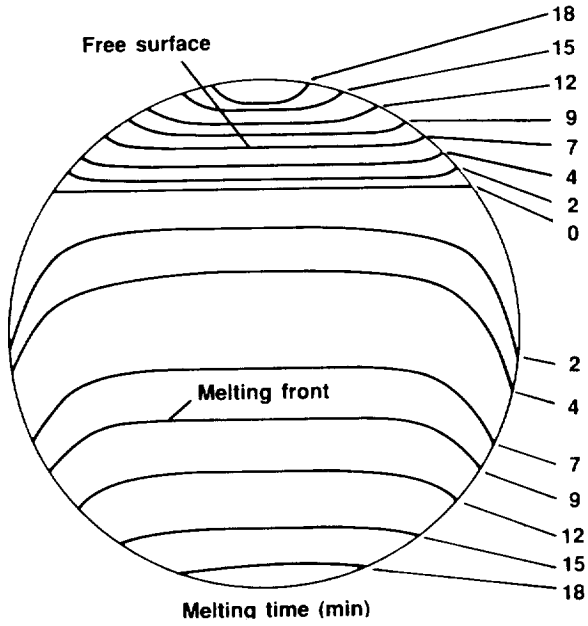


Figure 5. Position and shape of the melting front and the air-liquid free surface, $T_{w,o}$ = 66.4°C.

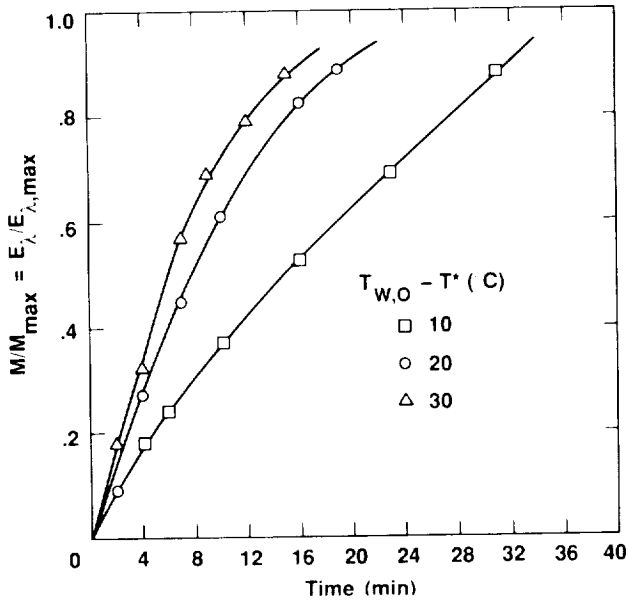


Figure 6. Melted mass and the energy of melting.

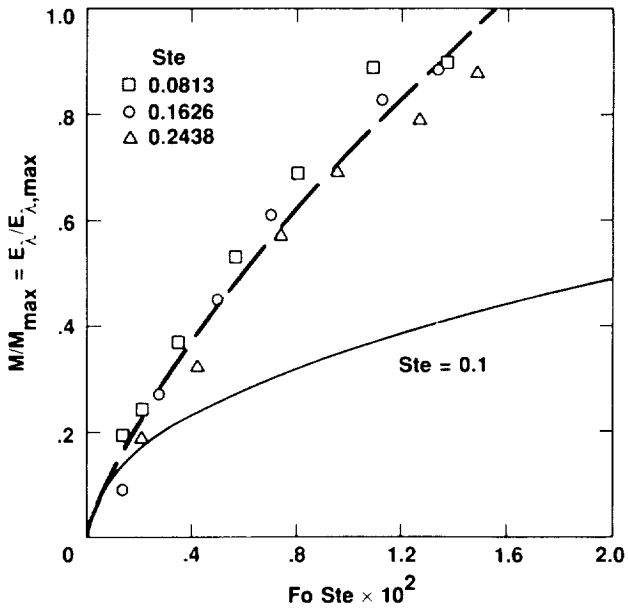


Figure 7. Correlation of data in figure 6 incorporated within heat conduction parameters and comparison with predictions of a one-dimensional heat conduction model.

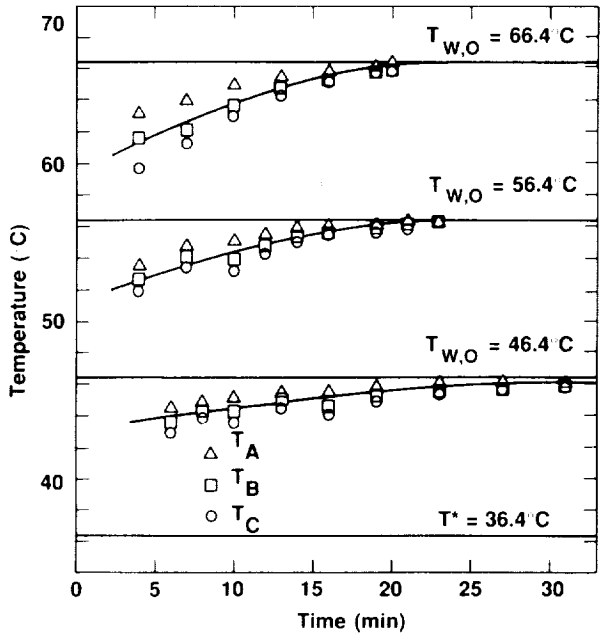


Figure 8. Timewise variation of the liquid melt temperature.

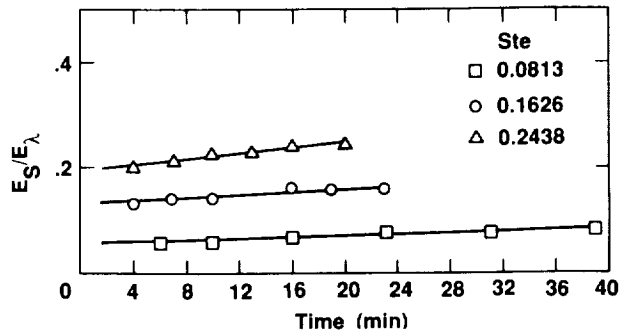


Figure 9. Comparison of the sensible energy stored in the liquid melt with the energy of melting.

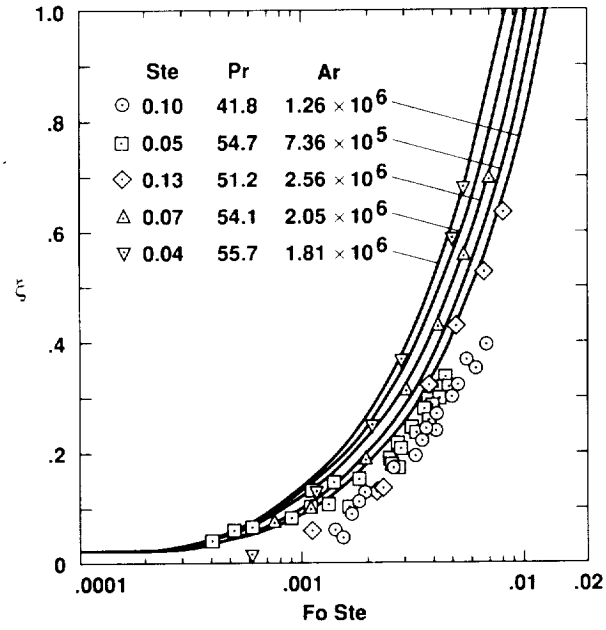


Figure 10. Comparison of analysis of reference 6 (solid curves) to experiments: square and circle symbols (ref. 4); triangles and diamonds, present experiments.

NASA
National Aeronautics and Space Administration

# Report Documentation Page

| 1. Report No. | 2. Government Accession No. | 3. Recipient's Catalog No. |
|---|---|---|
| NASA TM-102822 | | |

| 4. Title and Subtitle | 5. Report Date |
|---|---|
| Natural Melting Within a Spherical Shell | June 1990 |
| | 6. Performing Organization Code |

| 7. Author(s) | 8. Performing Organization Report No. |
|---|---|
| Parviz A. Bahrami | A-90155 |
| | 10. Work Unit No. 505-60-11 |

| 9. Performing Organization Name and Address | 11. Contract or Grant No. |
|---|---|
| Ames Research Center<br>Moffett Field, CA 94035-1000 | |
| | 13. Type of Report and Period Covered<br>Technical Memorandum |
| 12. Sponsoring Agency Name and Address | 14. Sponsoring Agency Code |
| National Aeronautics and Space Administration<br>Washington, DC 20546-0001 | |

15. Supplementary Notes

Point of Contact: Parviz A. Bahrami, Ames Research Center, MS T045-2
Moffett Field, CA 94035-1000 (415) 604-4964 or FTS 464-4964

16. Abstract

Fundamental heat transfer experiments were performed on the melting of a phase-change medium in a spherical shell. Free expansion of the medium into a void space within the sphere was permitted. A step function temperature jump on the outer shell wall was imposed and the timewise evolution of the melting process and the position of the solid-liquid interface was photographically recorded. Numerical integration of the interface position data yielded information about the melted mass and the energy of melting. It was found that the rate of melting and the heat transfer were significantly affected by the movement of the solid medium to the base of the sphere due to gravity. The energy transfer associated with melting was substantially higher than that predicted by the conduction model. Furthermore, the ratio of the measured values of sensible energy in the liquid melt to the energy of melting were nearly proportional to the Stefan number. The experimental results are in agreement with our theory set forth in an earlier paper.

| 17. Key Words (Suggested by Author(s)) | 18. Distribution Statement |
|---|---|
| Phase change<br>Melting<br>Gravity-controlled melting<br>Microgravity heat transfer | Unclassified-Unlimited<br>Subject Category – 34 |

| 19. Security Classif. (of this report) | 20. Security Classif. (of this page) | 21. No. of Pages | 22. Price |
|---|---|---|---|
| Unclassified | Unclassified | 20 | A02 |

NASA FORM 1626 OCT 86

For sale by the National Technical Information Service, Springfield, Virginia 22161